Band-edge states in short-period $(GaAs)_m/(AlAs)_n$ superlattices

Sudha Gopalan,* N. E. Christensen, and M. Cardona
Max-Planck-Institut für Festkörperforschung, Heisenbergstrasse 1, Postfach 80 06 65, D-7000 Stuttgart 80, Federal Republic of Germany
(Received 11 July 1988)

We investigate the character of the electron and hole states in [001]-stacked $(GaAs)_m/(AlAs)_n$ superlattices with $m,n \leq 3$ by means of the first-principles linear–muffin-tin-orbital method. The highest valence states are found to localize more on the GaAs layers with increasing superlattice period, while the lowest conduction states at the Γ point are confined in the AlAs region in most cases. The calculated gaps (direct and indirect) compare well with experimental results. The heavy-hole- and light-hole-like states, split by the tetragonal perturbation of the superlattice, exhibit dispersions with strong nonparabolicities related to anticrossing of states for values of $\mathbf{k}$ close to the Γ point, and spin splittings along the superlattice layers. The effective masses of holes and electrons are calculated at the Γ point and are found to show little variation within themselves. The spin splittings are accounted for by $\mathbf{k}$-linear terms. A semiempirical $\mathbf{k}\cdot\mathbf{p}$ perturbation theory is developed for the two highest valence states, the parameters of which are obtained by a fit to the first-principles bands.

I. INTRODUCTION

Compositional superlattices consisting of alternating layers of different semiconductors have attracted a great deal of experimental and theoretical interest. One of the fundamental questions in the study of these systems is how the presence of a new periodicity normal to the layers manifests itself in the character of the electron and the hole states. Superlattices grown with GaAs and AlAs, which have similar lattice parameters but significantly different fundamental energy gaps, constitute a prototype for such studies. These superlattices with large periods ($\gtrsim 60$ Å) are of type I where the electrons and holes at the band edges are confined in the GaAs layers by the barrier potential of the AlAs layers. One has then the familiar multiple-quantum-well structure,[1] where the motion of the electrons and holes normal to the layers is quantized while the motion along the layer is of two-dimensional character.[1] However, as the superlattice period is decreased with the GaAs layer ≤ 30 Å and the AlAs layer of the same thickness or larger, the superlattice switches from type I and type II, where the electrons and holes are spatially separated.[2] The electrons are no longer bound in the GaAs layers but are identified as those associated with the X state in AlAs.

The electronic structures of these superlattices have been studied theoretically in great detail by an envelope-function approach[3–9] in which each layer is considered like a macroscopic crystal modified at most by a slowly varying potential. The wave functions can then be written in the form of amplitude-modulated Bloch waves with slowly varying envelope functions satisfying definite boundary conditions. Thus the basic ingredients of this approach are the bulk band structures of the two layers in a suitably parametrized form ($\mathbf{k}\cdot\mathbf{p}$) and the appropriate band offsets. This has been successfully used to study many interesting problems such as effects of modulation doping, band mixing, and excitonic interaction.[5–8] Other approaches involving a full three-dimensional band-structure calculation include the tight-binding schemes[2,10–12] and the empirical pseudopotential methods.[13–15] These methods, although treating the boundary conditions in a more natural way, contain many empirical parameters which are obtained by a careful fit to experimental data of the bulk semiconductors constituting the superlattice.

It is the purpose here to address the topics of confinement effects and electronic structures of superlattices when the thicknesses of the alternating layers are reduced down to a few monolayers, where each monolayer has as thickness half the cubic lattice constant of bulk GaAs (~ 2.8 Å). The interaction between the particles in the different layers increases considerably and it becomes questionable to treat each layer using bulklike parameters. The empirical methods described before have been applied[10,13–16] to these very-short-period superlattice systems but provide many conflicting results when compared with each other. In order to obtain a more accurate description of these systems we therefore treat them as usual bulk crystals (with many atoms in the unit cell of the superlattice) and perform a first-principles band-structure calculation described in Sec. II. Naturally, no boundary conditions are required. We consider superlattices with a periodic stacking of m monolayers of GaAs and n monolayers of AlAs along the [001] direction, and restrict $m,n \leq 3$.

This microscopic description of the electronic states leads to several interesting features presented in Sec. III. The confinement of the valence-band top in the GaAs region increases drastically with superlattice period while the lowest conduction-band state is confined in most cases to the AlAs region. The location in the Brillouin zone of the conduction-band minima is established and

 ©1989 The American Physical Society

we find that most of the superlattices studied are indirect both in real and **k** space. The calculated gaps (direct and indirect) compare well with available experimental data. We have also calculated the effective masses of holes and electrons at the Γ point. The hole masses for all the superlattices treated differ considerably from the values of the bulk constituent but show little variation within themselves. The dispersion of heavy-hole- and light-hole-like states along the superlattice layers close to the Γ point exhibit spin splittings and strong nonparabolicities.

Other first-principle calculations have been performed for these ultrathin superlattices.[17–24] However, most of these have only addressed problems of stability and band offsets. In addition, the fine structure of the energy bands around the Γ point, which is of concern here, has not been examined before.

It is of great interest to study the effect of external fields such as magnetic field, electric field, and uniaxial stress on these very-short-period superlattices. Unfortunately, the first-principle calculations cannot treat these problems nor can the approaches used for thicker superlattices be extended to the present case due to the nonapplicability of bulklike parameters. We show in Sec. IV that treating the short-period superlattices considered here as bulk crystals we can expand the states around the band edges in a $\mathbf{k}\cdot\mathbf{p}$ form, the parameters of which can be extracted by fitting the first-principles bands. As an example we consider the four heavy-hole and light-hole states and reproduce their essential features around the Γ point using the $\mathbf{k}\cdot\mathbf{p}$ formalism.

II. FORMALISM

The electronic band structures of $(GaAs)_m/(AlAs)_n$ superlattices constructed along the [001] direction of bulk zinc-blende material, as shown in Fig. 1 for the $(GaAs)_1/(AlAs)_1$ case, are calculated here within the framework of the local density functional theory[25] by means of the self-consistent, relativistic linear–muffin-tin-orbital (LMTO) method.[26] Similar to the calculations of zinc-blende-type semiconductors, we include empty spheres, that is, atomic spheres with no net nuclear charge, in the empty tetrahedral sites in order to obtain a close-packed structure. The so-called combined correction term[26,27] is also taken into account.

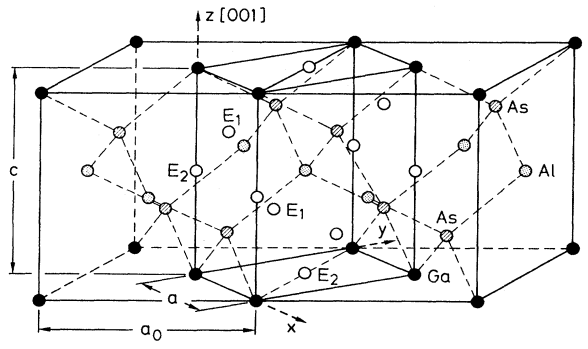

FIG. 1. Atomic positions and crystallographic directions for the monolayer superlattice constructed along the [001] zinc-blende lattice. The positions of the empty spheres E_1 and E_2 used for purpose of calculation are shown only in the superlattice unit cell.

The unit cells of superlattices with $(m+n)$=even having the space-group symmetry D_{2d}^1 (as shown in Fig. 1 for the monolayer case) are simple tetragonal with $c/a=(m+n)/\sqrt{2}$, while those with $(m+n)$=odd having the space-group symmetry D_{2d}^{11} are body-centered tetragonal with $c/a=(m+n)\sqrt{2}$, where c is the unit-cell dimension along the stacking direction ([001] here). The number of basis atoms (including empty spheres) in the unit cell is $4(m+n)$ for both cases. The positions of the atoms in the $(GaAs)_1/(AlAs)_1$ superlattice unit cell as indicated in Fig. 1 are

$$\begin{aligned}
&\text{Ga: } \frac{a}{2}(0,0,0), \quad \text{Al: } \frac{a}{2}\left[1,1,\frac{c}{a}\right], \\
&\text{As: } \frac{a}{2}\left[0,1,\frac{c}{2a}\right], \quad \text{As: } \frac{a}{2}\left[1,0,\frac{3c}{2a}\right], \\
&E_1\text{: } \frac{a}{2}\left[1,0,\frac{3c}{2a}\right]; \ \frac{a}{2}\left[0,1,\frac{c}{2a}\right], \\
&E_2\text{: } \frac{a}{2}\left[0,0,\frac{c}{a}\right]; \ \frac{a}{2}(1,1,0),
\end{aligned} \tag{1}$$

where E_1 and E_2 are the empty spheres surrounding the cations and anions, respectively. The positions of the atoms in larger unit cells for the other superlattices can be written down very easily by extending those presented in (1) for the $(GaAs)_1/(AlAs)_1$ case. We obtain $a=a_0/\sqrt{2}$, where a_0 is the (cubic) lattice constant of the constituent bulk materials. We take for a_0 the bulk GaAs value of $a_0=5.66$ Å. In addition, we assume no lattice mismatch between the superlattice layers. This is quite reasonable as the difference in the lattice constants of GaAs and AlAs is less than 0.2%. The Brillouin zone of superlattices with $(m+n)$=even is simple tetragonal while that for $(m+n)$=odd is body-centered tetragonal. In Fig. 2 the Brillouin zones for a few cases are drawn embedded in the parent zinc-blende Brillouin zone in order to describe zone foldings. For example, the X point (along the $\hat{\mathbf{k}}_z$ direction) of the fcc zone folds onto the Γ point for cases with $(m+n)$=even and onto the Z point for cases with $(m+n)$=odd. From Fig. 2(b) we notice that as we increase the number of layers the superlattice Brillouin zone is compressed along $\hat{\mathbf{k}}_z$ and is accompanied by increased zone foldings.

The wave functions in each atomic sphere (including empty ones) contain s, p, and d partial waves. We have included spin-orbit interaction in all the calculations as a perturbation to the scalar-relativistic Hamiltonian. Thus the Hamiltonian matrices involved in the computation are of dimension $72(m+n)$. This limits the procedure to rather restricted values of m and n. It is of particular importance to note that we have not treated the cation d states as ("frozen" renormalized) corelike states but as fully relaxed band states.[18,27] This is necessary because the d states hybridize with the valence-band maxima, and hence influence the band-offset values.[18]

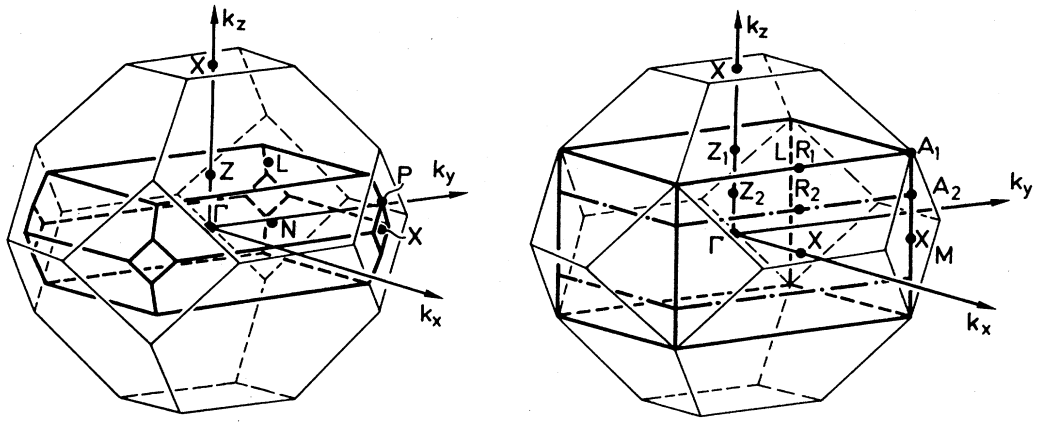

FIG. 2. Brillouin zone of superlattices (thick line) with (a) $(m+n)=3$ (odd) and (b) $(m+n)=2$ (even) embedded in the parent zinc-blende Brillouin zone. In (b) the Brillouin zone of the superlattice with $(m+n)=4$ is also drawn.

The crystal potentials are obtained by iterating the one-electron wave equation to self-consistency with an effective potential where exchange correlation treated in the local density approximation is of the form constructed by Ceperley and Alder[28] in a parametrized form.[29] This is known to produce gaps which are too small. We correct for this in the same way as done for bulk semiconductors[30] by adding external potentials $V_a(\mathbf{r})$ of the form

$$V_a(\mathbf{r})=V_0\left[\frac{r_0}{r}\right]e^{-(r/r_0)^2} \tag{2}$$

which are sharply peaked at each atomic site a. The values of the parameters V_0 and r_0 were chosen in Ref. 30 for the bulk zinc-blende semiconductors, such that the band gaps at the three symmetry points Γ, X, and L agree with experiments at 4 K. The values of V_0 and r_0 thus chosen for the different atoms in bulk GaAs and AlAs are retained here for all the superlattices; they are presented in Table I. The reasons for doing so are first, the lack of accurate knowledge of experimental gaps, and second, the fact that the strengths and lengths of the Ga—As and Al—As bonds are very similar and hence are not expected to undergo drastic changes in the superlattice. This represents an empirical way of correcting for the self-energy term.[31] These extra potentials are included in the final self-consistency runs. It should be noted that the valence states and the ground-state properties remain quite insensitive to these extra potentials.

TABLE I. Parameters V_0 (hartrees) and r_0 (bohrs) of the potentials [see Eq. (2)] added at the different sites to correct for the band gaps.

	Ga	Al	As	Empty sphere surrounded by cations E_1	Empty sphere surrounded by anions E_2
V_0	280.0	340.0	190.0	5.0	6.0
r_0	0.015	0.015	0.015	0.55	0.55

III. RESULTS AND DISCUSSION

A. Electronic structure

Equipped with this formalism, we calculated the band structure of $(GaAs)_m/(AlAs)_n$ superlattices in the [001] orientation with $m,n \leq 3$. The results of such a calculation along high-symmetry directions are presented in Fig. 3(a) for the $(GaAs)_2/(AlAs)_2$ superlattice with $(m+n)$ =even and in Fig. 3(b) for the $(GaAs)_1/(AlAs)_2$ superlattice with $(m+n)$=odd. The symmetry points in Fig. 3(a) referred to the tetragonal Brillouin zone [Fig. 2(b)] are $\Gamma=(\pi/a)(0,0,0)$, $R=(\pi/a)(1,0,a/2)$, $A=(\pi/a)(1,1,a/c)$, $Z=(\pi/a)(0,0,a/c)$, $M=(\pi/a)(1,1,0)$, and $X=(\pi/a)(1,0,0)$ and those in Fig. 3(b) referred to the body-centered tetragonal Brillouin zone [Fig. 2(a)] are $N=(\pi/a)(1,0,a/c)$, $X=(\pi/a)(1,1,0)$, $p=(\pi/a)(1,1,a/c)$, and $Z=(\pi/a)(0,0,2a/c)$. The energies are referred to the natural scale in the atomic sphere approximation in which the Coulomb potential of the atomic spheres is zero at infinity.[26] The gross features of the valence-band structures calculated (see Fig. 3) are the dispersionless Ga $3d$ bands around -16 eV [these states have not been shown in Fig. 3(b)]. The As $3d$ bands (not shown in Fig. 3) lie at about 11 eV below the Ga $3d$ states and are treated as frozen core states. The As s bands lie around -12 eV and the broad band from about -1 to -7 eV consists mainly of Ga p, Al p, and As p states. The total widths and gaps of valence bands are comparable with those of the constituent materials, namely bulk GaAs and AlAs. Similar bands for $(GaAs)_1/(AlAs)_1$ along a few symmetry directions have been given in Ref. 32.

The valence-band top, which is of particular interest here, consists mainly of the anion (As) p states like in bulk semiconductors. However, in these superlattices the anion bonds (As p) are shared between Ga and Al atoms and hence it is important to find out the nature of the As state (i.e., the confinement effects) at the valence-band maxima. This is done by analyzing the angular momentum composition of the wave functions around each of the atomic spheres. The results are presented in Fig. 4 as

the relative As p contribution (in percent) to the valence-band maxima originating from each layer of the superlattice. The dots in Fig. 4 are the values obtained from the present *ab initio* calculation while the dashed lines are just guides to the eye. In the $(GaAs)_1/(AlAs)_1$ superlattice the As originating from both GaAs and AlAs layers contributes equally to the valence-band top. However, this situation changes drastically as the superlattice thickness is increased where we observe an increasing contribution from the GaAs layers. A similar calculation for the $(GaAs)_7/(AlAs)_7$ superlattice, shown in the lowest plot in Fig. 4, indicates that the valence-band top is almost completely confined to the GaAs region. Similar analysis can be applied to the lower valence-band states and we can identify states confined in the AlAs region or in the interface region. These conclusions support the application of the envelope-function-type approaches to the thicker-period superlattices but not to the very short ones. Similar conclusions have been drawn by other first-principles methods.[21,24]

The conduction bands also show interesting confinement features. As indicated earlier [Fig. 2(b)], in superlattices with $(m+n)$=even the X point (along $\hat{\mathbf{k}}_z$) of the bulk fcc zone folds over to the Γ point of the superlattice zone. Since the X conduction band of AlAs is lower than the Γ conduction band of GaAs it has been conjectured[33–35] that the conduction-band edge at the Γ point in these superlattices is an X-like AlAs band. Analysis of the wave functions of the present calculations indicates that this is indeed true for cases with $m=n$ (with the exception of the $m=n=1$ case), and for others with $m\neq n$ having larger AlAs content. This is clearly seen in Table II where we have presented the two minimum Γ gaps, one Γ_6^c arising from the normal Γ-like GaAs band (E_0) and the other Γ_X^c from the folded X_3-like AlAs band (E_{0X}) in the case $(m+n)$=even and from points along Δ (see Table II) close to X for $(m+n)$=odd. For $m=n$ a systematic decrease of E_{0X} with increasing m is found while some fluctuations are found in the gaps for $m\neq n$. In the case $(m+n)$=odd we usually find larger E_{0X} gaps than for the closest $(m+n)$=even superlattices, which is expected from the fact that in the former case the gaps correspond to points *inside* of the large zone (not at X). In this case the difference between (m,n) and (n,m) gaps decreases with increasing $m+n$ as the corresponding Δ point approaches X.

In Table II we have also listed the indirect energy gaps E_g smaller than the Γ gaps, along with the location in the Brillouin zone of the conduction bands (the valence-band top is always at Γ). The lowest gap falls in the range 1.8 ± 0.12 eV and fluctuates as it switches from one point of the Brillouin zone to another, a fact which is not surprising in view of the small range of energies involved. From a numerical point of view we believe that these fluctuations are meaningful. However, they may not be from a physical viewpoint as a result of systematic errors in the method, in particular the way of treating the "gap problem."

All these energies have been listed in order to facilitate comparison with different experimental data.[33–39] Optical excitations across the gap are dominated by pairs of

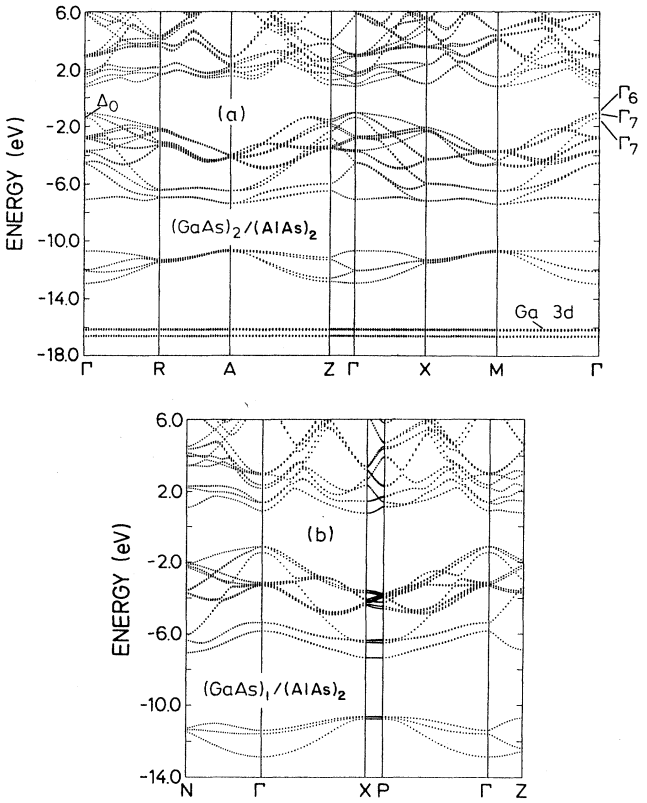

FIG. 3. Energy-band structure of $(GaAs)_m/(AlAs)_n$ superlattices in the [001] orientation with (a) $(m+n)$=even and (b) $(m+n)$=odd. The various symmetry points for the two cases are indicated in Fig. 2. The dispersionless Ga $3d$ states are not shown in (b).

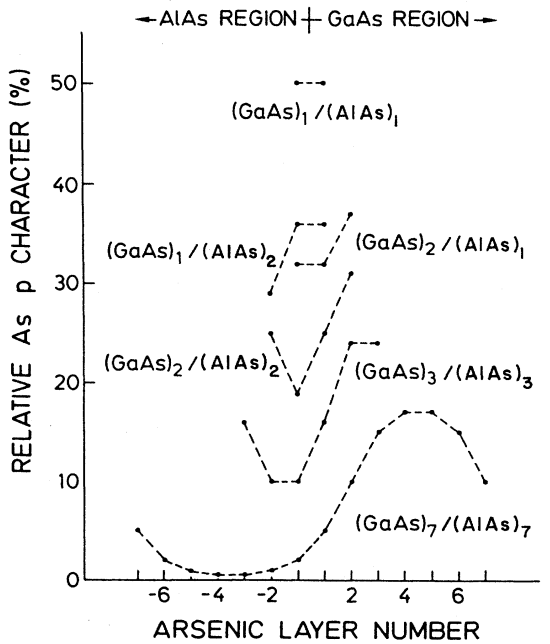

FIG. 4. Relative contribution (in percent) of the As p states to the valence-band maxima from each layer for different superlattices.

states coupled by large momentum matrix elements. Structure factor considerations dictate that such matrix elements be small for transitions between nonfolded and folded states. These have also been evaluated explicitly in the present scheme for the purpose of calculating optical-absorption spectra.[40] Thus optical-excitation and -absorption measurements[33–38] would detect the $E_0(\Gamma_6^v-\Gamma_6^c)$ gaps between nonfolded states even though they may not be the smallest gap at the Γ point. It is the minimum energies E_g which should be considered in interpreting luminescence data.[33–35,39] Similar calculations performed on the $(GaAs)_7/(AlAs)_7$ system indicate that the lowest conduction-band state is still the folded X-like AlAs state. Thus all superlattices studied up to $m=n=7$ are of type II. The $(GaAs)_1/(AlAs)_1$ is the only exception with the X-like AlAs state lying 0.06 eV above the Γ-like GaAs state. However, this energy difference is very small, and a definite conclusion regarding the ordering cannot be made for this case. Calculations are presently being extended to larger systems in order to determine the critical periodicity where the superlattice switches from type II to type I.

B. Symmetry considerations

We now consider the changes in the valence-band symmetries in going from the point group T_d of bulk zinc-blende semiconductors to the D_{2d} point group describing the superlattice. The p-like valence-band top in bulk GaAs in the presence of spin-orbit interaction consists of the fourfold degenerate Γ_8 states and a twofold degenerate Γ_7 split-off state. In the angular momentum representation (j,m_j) with [001] as the quantization direction the Γ_8 states are the four $(\frac{3}{2},\pm\frac{3}{2})$ and $(\frac{3}{2},\pm\frac{1}{2})$ states while the Γ_7 are the $(\frac{1}{2},\pm\frac{1}{2})$ states. For $\mathbf{k}\neq\mathbf{0}$, a splitting of the heavy-hole $(\frac{3}{2},\pm\frac{3}{2})$ states from the light-hole $(\frac{3}{2},\pm\frac{1}{2})$ states occurs.

On the other hand, using the notations and character table of Ref. 41 we find that in the point group symmetry D_{2d} of the superlattice the p-like valence-band top transforms like the three doubly degenerate states Γ_6, Γ_7, and Γ_7. Thus the most obvious change is a splitting of the fourfold degenerate Γ_8 states in, say, bulk GaAs into two twofold degenerate states Γ_6 and Γ_7 in the superlattice. This is the splitting Δ of the heavy-hole and light-hole

TABLE II. The two minimum Γ gaps E_0 and E_{0X}, spin-orbit splittings Δ_0, heavy-hole and light-hole splittings Δ, the minimum (indirect) energy gaps E_g, and experimental gaps for different superlattices. The position in the Brillouin zones of the lowest conduction-band state is indicated in parentheses. The bulk values are from Ref. 46.

Superlattices period (m,n)	Δ (eV)	Δ_0 (eV)	Band gaps at Γ point $E_0=E\lvert\Gamma_6^v-\Gamma_6^c\rvert$ (eV)	$E_{0X}=E\lvert\Gamma_6^v-\Gamma_x^c\rvert$ (eV)	E_g (eV)	Experimental results (eV)
(1,1)	0.021	0.34	1.93	1.99	1.69 (R)	2.35,[a] 2.24,[b] 2.27,[c] 2.006,[d] 2.108,[e] 2.086,[f] 1.931,[g] 1.890,[h] 2.05[i]
(2,1)	0.013	0.35	1.74	2.12[j]		1.83,[a] 1.84,[c] 1.815,[f] 1.845[d]
(1,2)	0.012	0.33	2.03	2.50[j]	1.88 (X) 1.92 (Z)	2.48,[a] 2.53,[c] 2.101[f]
(2,2)	0.012	0.34	2.03	1.85		2.19,[a] 2.190,[b] 2.08,[c] 2.070,[f] 1.971,[g]2.02[i]
(3,1)	0.012	0.36	1.66	1.93	1.62 (X)	1.82,[c] 1.776[f]
(1,3)	0.011	0.33	2.30	1.91	1.89 (M)	2.59,[a] 2.60,[c] 2.127[f]
(3,2)	0.014	0.35	1.76	1.96[k]		
(2.3)	0.016	0.34	2.13	1.88[k]	1.83 (Z) 1.86 (X)	
(3,3)	0.022	0.34	1.97	1.79	1.77 (Z)	2.114,[b] 2.120,[l] 2.07,[c] 2.035,[h] 2.031[g]
bulk GaAs	0	0.34	1.52			
bulk AlAs	0	0.28	3.13		2.23	

[a]Excitation spectra of luminescence from Ref. 33 (4.6 K).
[b]Excitation spectra of luminescence from Ref. 34 (2 K).
[c]Ellipsometric results of Ref. 36 (30 K).
[d]Resonant Raman measurements of Ref. 37 (300 K).
[e]Resonant Raman measurements of Ref. 38 (300 K).
[f]Photoluminescence data of Ref. 33 (4.6 K).
[g]Photoluminescence data of Ref. 34 (2 K).
[h]Photoluminescence data of Ref. 35 (1.7 K).
[i]Photoluminescence data of Ref. 39 (4 K).
[j]This gap corresponds to the folded point along Δ $(4\pi/3)$ (001) and not to the X point.
[k]This gap corresponds to the folded point along Δ $(8\pi/5)$ (001) and not to the X point.
[l]Excitation spectra of luminescence from Ref. 35 (1.7 K).

states, induced by the tetragonal perturbation of the superlattice even at the Γ point, in addition to the spin-orbit splitting Δ_0. The values of Δ and Δ_0 (measured from the average heavy-hole and light-hole levels) are presented in Table II; they do not change much with superlattice period. Using the coupling coefficients of Ref. 41 we describe the six valence states as

$$\Gamma_6^{1/2}=\frac{1}{\sqrt{2}}(x-iy)\downarrow\ ,$$
$$\Gamma_6^{-1/2}=\frac{1}{\sqrt{2}}(x+iy)\uparrow\ , \tag{3}$$

$$\Gamma_7^{1/2}=\frac{1}{\sqrt{2}}(x+iy)\downarrow,\ \text{or}\ -z\uparrow\ ,$$
$$\Gamma_7^{-1/2}=\frac{1}{\sqrt{2}}(x-iy)\uparrow,\ \text{or}\ z\downarrow\ . \tag{4}$$

Transforming to the (j,m_j) representation it is straightforward to see that the Γ_6 states behave as $(\frac{3}{2},\pm\frac{3}{2})$ while the Γ_7 states have mixed $(\frac{3}{2},\pm\frac{1}{2})$, $(\frac{1}{2},\pm\frac{1}{2})$ character even at $\mathbf{k}=\mathbf{0}$. Away from $\mathbf{k}=\mathbf{0}$ the Γ_6 and Γ_7 bands ($m_j=\pm\frac{3}{2}$ and $\pm\frac{1}{2}$) are completely mixed.

C. Effective masses of holes and electrons

In order to study the finer structures around $\mathbf{k}=\mathbf{0}$, we divide the Brillouin-zone segments along [100], [110], and [001] directions using a dense k mesh of up to 1000 points. We calculate the electronic energies for about 30 such points around $\mathbf{k}=\mathbf{0}$, the results of which are shown in Fig. 5 for the two highest valence bands [heavy-hole (Γ_6) and light-hole (Γ_7) states] of a $(GaAs)_2/(AlAs)_2$ superlattice along the [110], [100], and [001] directions. We notice that the bands along [100] and [110] directions exhibit special features such as nonparabolicities related to anticrossing of states for values of $\mathbf{k}$ close to the Γ point and spin splittings. The bands along [001] show no such mixing or spin splittings, as displayed in Fig. 5 for the $(GaAs)_2/(AlAs)_2$ superlattices. It should be noted, however, that all other superlattices studied exhibit similar features. It would be interesting to observe effects of these band mixings experimentally like those reported for larger-period superlattices.[42–44]

By fitting parabolas to the calculated bands shown in Fig. 5 in the immediate neighborhood of $\mathbf{k}=\mathbf{0}$ the effective hole masses can be obtained along the different directions. These are presented in Table III together with the masses of the spin-orbit-split band. The transverse masses, that is, masses calculated along [100] and [110], are nearly isotropic and are given in Table III as perpendicular ($\perp$) masses while the longitudinal mass calculated along [001] is presented in Table III as the parallel ($\parallel$) mass for the different superlattices considered here. We observe that these hole masses remain more or less constant with superlattice period but are considerably changed from the constituent bulk values also presented in Table III. The hole masses of bulk GaAs are those calculated in Ref. 30 using the same scheme followed here while the hole masses of bulk AlAs are taken from Ref. 45. We observe that for directions *parallel* ($\parallel$) to the superlattice growth direction, [001], the heavy-hole band has an effective mass larger than that of the light-hole band while this situation is reversed for directions *perpendicular* to [001] ($\perp$). These results are similar to those obtained when a uniaxial tensile stress is applied along [001] to bulk zinc-blende crystals, reducing the symmetry from T_d to D_{2d}. In this case the upper bands are heavier than the lower ones along the direction of stress but lighter along the perpendicular direction while the spin-orbit-split bands remain nearly isotropic.[46]

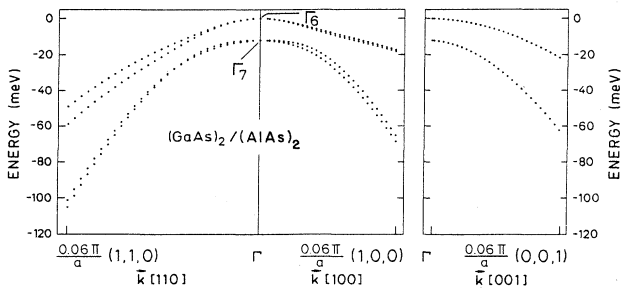

FIG. 5. Dispersion of the heavy-hole and light-hole states close to the Γ point for $(GaAs)_2/(AlAs)_2$ superlattice along the direction [110], [100], and [001] as calculated with the LMTO method.

The effective masses of electrons in the two lowest conduction bands at the Γ point calculated along directions parallel and perpendicular to the growth direction are also presented in Table III. The bands which are identified as folded bands (see Table II) are characterized by heavier effective masses and some have even negative, that is holelike, masses. The effective masses of Γ_6 electrons arising from the normal Γ_6-like GaAs state are almost isotropic and approximately scale according to the gap of the state. However, some of the masses along the growth direction are found to be very large. This may be due, as discussed in Ref. 47, to a large mixing from the higher-lying states.[48] It should be borne in mind that all the conclusions drawn for the conduction-band electrons depend sensitively on the details of the correction used for the band gaps. There are no experimental data for these electron and hole masses in the superlattices considered. These masses have been calculated in Ref. 23 for the $(GaAs)_m/(AlAs)_n$ superlattices using the linearized-augmented-plane-wave method and they obtain composition-dependent masses for both holes and electrons. This is in contrast to the conclusions drawn here. Calculations are under way for larger unit cells using the present scheme to study the changes in their effective masses.

D. Spin splittings

As mentioned earlier, all states perpendicular to the superlattice growth direction exhibit spin splittings as shown for the heavy-hole and light-hole states in Fig. 5 for the $(GaAs)_2/(AlAs)_2$ superlattice. These spin splittings can be explained by a linear spin-orbit term for crystals with the D_{2d} point group symmetry. In simplest terms such as interaction can be written in the form

TABLE III. The effective masses of the heavy-hole, light-hole, spin-orbit hole, and the two lowest conduction states at Γ calculated along the directions parallel (||) and perpendicular (⊥) to the growth direction ([001]). The nature of the electron states can be identified from the Γ gaps presented in Table II.

Superlattice period (m,n)	$\left[\frac{m^*}{m_0}\right]_{hh}$ ⊥	$\left[\frac{m^*}{m_0}\right]_{hh}$ ||	$\left[\frac{m^*}{m_0}\right]_{lh}$ ⊥	$\left[\frac{m^*}{m_0}\right]_{lh}$ ||	$\left[\frac{m^*}{m_0}\right]_{sh}$ ⊥	$\left[\frac{m^*}{m_0}\right]_{sh}$ ||	$\left[\frac{m^*}{m_0}\right]_{c_1}$ ⊥	$\left[\frac{m^*}{m_0}\right]_{c_1}$ ||	$\left[\frac{m^*}{m_0}\right]_{c_2}$ ⊥	$\left[\frac{m^*}{m_0}\right]_{c_2}$ ||
(1,1)	0.186	0.376	0.248	0.168	0.268	0.252	0.146	−0.216	0.260	0.072
(2,1)	0.192	0.352	0.202	0.142	0.240	0.230	0.118	0.128	0.236	−0.458
(1,2)	0.234	0.406	0.252	0.180	0.286	0.276	0.160	0.328	0.186	−0.050
(2,2)	0.202	0.384	0.236	0.160	0.264	0.254	0.214	0.518	0.144	0.176
(3,1)	0.160	0.338	0.216	0.132	0.230	0.220	0.108	0.128	0.254	0.722
(1,3)	0.220	0.420	0.296	0.190	0.298	0.290	0.256	4.442	0.170	0.180
(3,2)	0.160	0.380	0.244	0.150	0.254	0.244	0.162	0.234	0.162	0.344
(2,3)	0.200	0.420	0.278	0.176	0.284	0.274	0.252	−1.000	0.144	0.150
(3,3)	0.200	0.432	0.252	0.170	0.278	0.264	0.254	−1.094	0.132	0.124
bulk GaAs	0.61		0.096		0.20		0.068			
bulk AlAs	0.5		0.26		0.37		0.124			

$$H_1=\alpha\sigma\cdot(\omega\times\mathbf{k}) , \tag{5}$$

where ω is any vector field with the full symmetry of the superlattice, α is a constant, and σ and $\mathbf{k}$ are the spin and momentum operators, respectively.

In Fig. 6(a) we present the spin splittings for the three highest valence bands as a function of $\mathbf{k}$ close to Γ. Similar plots for the two lowest conduction states are shown in Fig. 6(b). The slopes of these curve at $\mathbf{k}=\mathbf{0}$ determine the constant α in Eq. (5) for a given choice of ω. The spin splittings can also be characterized by their slopes C. The values obtained for these slopes from the data shown in Fig. 6 are (in atomic units)

$$C_{hh}=5.56\times10^{-4},\quad C_{c_1}=3.01\times10^{-3} ,$$
$$C_{lh}=1.50\times10^{-2},\quad C_{c_2}=5.79\times10^{-3} , \tag{6}$$
$$C_{sh}=1.31\times10^{-2} ,$$

where the subscripts hh, lh, sh, c_1, and c_2 refer to the heavy hole (v_1), light hole (v_2), spin-orbit hole (v_3), and the two lowest electron states c_1 and c_2 at the Γ point. We find that for the heavy-hole bands the linear term is extremely small. The spin splittings for bulk materials have been described in detail in Ref. 49.

IV. k·p ANALYSIS

For the interpretation of the most experimental data a detailed knowledge of the wave functions and the energy levels throughout the Brillouin zone is not necessary. However, a description of the states around certain special points (particularly the Γ point) of energy bands is needed in terms of certain semiempirical parameters such as effective masses. This also facilitates the study of the evolution of these states under external perturbations. Thus we develop a semiempirical $\mathbf{k}\cdot\mathbf{p}$ perturbation theory for short-period superlattices.

We consider here the two highest valence bands, the heavy-hole (Γ_6) and the light-hole (Γ_7) states [Eqs. (3)

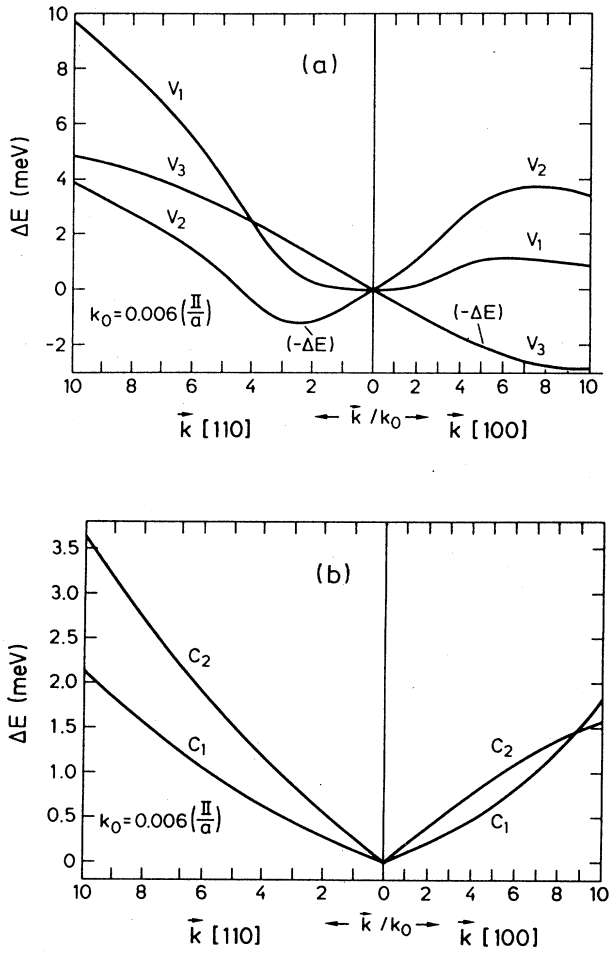

FIG. 6. Spin splittings of the (a) heavy-hole (v_1), light-hole (v_2), and spin-orbit-split hole states and (b) the two lower conduction-band states for $(GaAs)_2/(AlAs)_2$ superlattices close to $\mathbf{k}=\mathbf{0}$ along the [110] and [100] directions as calculated with the LMTO method.

and (4)] around $\mathbf{k}=\mathbf{0}$. We neglect coupling to the spin-orbit-split band here as we are considering energies much less than the spin-orbit splitting of about 350 meV. We include linear terms as described by Eq. (5). We obtain for the representations of the group D_{2d} the products[41] $\Gamma_6\times\Gamma_6=\Gamma_1+\Gamma_2+\Gamma_5$, $\Gamma_6\times\Gamma_7=\Gamma_3\times\Gamma_4\times\Gamma_5$, and $\Gamma_7\times\Gamma_7=\Gamma_1+\Gamma_2+\Gamma_5$ and using the basis functions for these representations we can write the $\mathbf{k}\cdot\mathbf{p}$ Hamiltonian for the four basis states $\Gamma_6^{1/2}$, $\Gamma_7^{-1/2}$, $\Gamma_7^{1/2}$, and $\Gamma_6^{-1/2}$ as

$$H=\begin{bmatrix} a_h & b-l_1 & c-l_2 & l_3 \\ b^*-l_1^* & a_l & l_4 & c+l_2 \\ c^*-l_2^* & l_4^* & a_l & -b+l_1 \\ l_3^* & c^*+l_2^* & -b^*+l_1^* & a_h \end{bmatrix}, \tag{7}$$

where

$$\begin{aligned} a_h &= E_h-\frac{\lambda_1}{2}k_z^2-\frac{\lambda_2}{2}(k_x^2+k_y^2)\ , \\ a_l &= E_l-\frac{\lambda_1'}{2}k_z^2-\frac{\lambda_2'}{2}(k_x^2+k_y^2)\ , \\ b &= \lambda_5(k_x+ik_y)k_z\ , \\ c &= \frac{\lambda_3}{2}(k_x^2-k_y^2)+i\lambda_4 k_x k_y\ , \end{aligned} \tag{7a}$$

and the linear terms, obtained from Eq. (5), are

$$\begin{aligned} l_1 &= C_1'(k_x-ik_y)\ , \\ l_2 &= C_2'k_z\ , \\ l_3 &= C_1(k_x+ik_y)\ , \\ l_4 &= C_2(k_x-ik_y)\ . \end{aligned} \tag{7b}$$

Here E_h and E_l are the energies at $\mathbf{k}=\mathbf{0}$ of the Γ_6 and Γ_7 states, respectively, and λ_1, λ_1', λ_2, λ_2', λ_3, λ_4, λ_5, C_1', C_2', C_1, and C_2 are constants to be determined.

The results of the first-principles calculations presented in the preceding sections indicate that the superlattices studied behave as bulk crystals. In addition the fine structures of the valence bands, obtained very accurately in the present scheme, are fairly similar for the different superlattices considered. Hence we can combine these results with the $\mathbf{k}\cdot\mathbf{p}$ model of Eq. (6) to extract the values of the parameters.

We notice that along the superlattice growth direction [001], the heavy-hole and light-hole states decouple with no mixing or spin splittings and with effective masses $1/\lambda_1$ and $1/\lambda_1'$, respectively. The dispersions parallel to the layers are, however, characterized by mixing and spin splittings. In Ref. 48 the linear terms were neglected and the dispersions parallel and perpendicular to the layers were combined with the simplified (2×2) $\mathbf{k}\cdot\mathbf{p}$ model to obtain the values of the parameters listed in Table IV. The same set of λ's was used in Ref. 48 to obtain good fits for all superlattices.

For bulk zinc-blende materials a $\mathbf{k}\cdot\mathbf{p}$ Hamiltonian similar to that presented in Eq. (7) is obtained with the constants replaced by functions of the Luttinger parameters γ_1, γ_2, and γ_3 as shown in parentheses in Table IV. The corresponding values for bulk GaAs and AlAs are presented in this table. They were obtained by using[7,45] $\gamma_1=6.85$, $\gamma_2=2.1$, and $\gamma_3=2.9$ for the Luttinger parameters for GaAs and $\gamma_1=3.45$, $\gamma_2=0.68$, and $\gamma_3=1.29$ for AlAs. The linear terms C_1 and C_2 give rise to the spin splittings of the heavy-hole and light-hole states [Eq. (6)]. The terms C_1' and C_2' are only important in the coupling region and hence can be neglected for small $\mathbf{k}$. We note that the bulk materials also exhibit splittings linear in k except for $\mathbf{k}$ along $\langle 100\rangle$.[49] These splittings, however, are much smaller than those seen in Fig. 6, with the exception of that of the v_1 band. In fact, in the bulk materials the splitting vanishes for the lowest conduction band at Γ. The lh and sh bands of the bulk materials, however, have large spin splittings which are proportional to k^3 for small k, the proportionality factors γ being given in Table VII of Ref. 49. These factors can be used to estimate linear terms in the superlattices if we take into account that confinement along z generates a spread in k_z (we label it Δk_z) which contributes two powers of k to the γk^3 splitting. We thus find[50]

$$\Delta E=\gamma k(\Delta k_z)^2\ , \tag{8}$$

where k is the magnitude of the $\mathbf{k}$ component in the x,y plane. Using the values of γ calculated with the LMTO method for GaAs and given in Table VII of Ref. 49 we find from the $C_{\rm lh}$, $C_{\rm sh}$, and C_{c_2} of Eq. (6) $\Delta k_z\cong 4\times10^{-2}$ bohr^{-1}, considerably smaller than that which would correspond to complete confinement in one of the constituent layers ($\Delta k_z=0.3$ bohr^{-1}). This confirms the weak confinement of band-edge states in the $(\mathrm{GaAs})_2/(\mathrm{AlAs})_2$ superlattice (see Fig. 4).

From the linear splittings given in Ref. 49 for bulk GaAs we find for the heavy-hole bands $C_{\rm hh}=6.2\times10^{-4}$ a.u. in rather good agreement with the value calculated

TABLE IV. The valence-band parameters for the short-period superlattices obtained by means of the LMTO method. The corresponding bulk GaAs and AlAs values are also shown.

Valence-band parameter		$(\mathrm{GaAs})_m\vert(\mathrm{AlAs})_n$ $m,n\le3$	GaAs	AlAs
λ_1	$(\gamma_1-2\gamma_2)$	5.2	2.65	2.09
λ_1'	$(\gamma_1+2\gamma_2)$	12.0	11.05	4.81
λ_2	$(\gamma_1+\gamma_2)$	10.0	8.95	4.13
λ_2'	$(\gamma_1-\gamma_2)$	8.2	4.75	2.77
λ_3	$(\sqrt{3}\gamma_2)$	6.2	3.64	1.18
λ_4	$(\sqrt{3}\gamma_3)$	3.1	5.02	2.23

from the data of Fig. 6 [$C_{hh}=5.56\times10^{-4}$, Eq. (6)]. The small linear splitting of the hh band in the superlattice thus mainly arises from coupling to the *d*-like core levels of Ga as in bulk GaAs.[49]

V. CONCLUSION

In conclusion, the first-principles LMTO method has provided some detailed features of the band-edge states in $(GaAs)_m/(AlAs)_n$ superlattices with $m,n<4$. The effective masses of electrons and holes calculated at the Γ point should serve as useful parameters in the interpretation of many experimental data. The strong nonparabolicities of the heavy-hole and light-hole states found for dispersions along the superlattice layers is explained in terms of mixing between these states. The spin splittings are explained by the presence of **k** linear terms.

The lowest conduction states in the $(GaAs)_m/(AlAs)_n$ superlattices are found to localize in the AlAs region for the cases with $m\leq n\leq7$. Most of the short-period superlattices studied here have therefore gaps that are indirect in real space, i.e., the electrons and holes are confined to different regions, and in reciprocal space. The semiempirical **k·p** theory developed to describe the dispersions of the heavy-hole and light-hole states around Γ should be useful in predicting the behavior of those states when external perturbations (e.g., magnetic, electric fields, uniaxial stress, and impurities) are applied and also for calculations of excitonic states.

*Present address: Department of Physics, The University of Western Ontario, London, Ontario, Canada N6A 3K7.

[1]R. Dingle, in *Festkörperprobleme (Advances in Solid State Physics)*, edited by H. J. Queisser (Vieweg, Braunschweig, 1975), Vol. XV, p. 21.
[2]J. Ihm, Appl. Phys. Lett. **50**, 1068 (1987).
[3]S. S. Nedorezo, Fiz. Tverd. Tela (Leningrad) **12**, 2269 (1971) [Sov. Phys.—Solid State **12**, 1814 (1971)].
[4]G. Bastard, Phys. Rev. B **25**, 7584 (1982).
[5]D. A. Broido and L. J. Sham, Phys. Rev. B **31**, 888 (1985).
[6]G. D. Sanders and Y. C. Chang, Phys. Rev. B **32**, 5517 (1985).
[7]M. Altarelli, U. Ekenberg, and A. Fasolino, Phys. Rev. B **32**, 5138 (1985).
[8]T. Ando, J. Phys. Soc. Jpn. **54**, 1528 (1985).
[9]D. L. Smith and C. Mailhiot, Phys. Rev. B **33**, 8345 (1986); **33**, 8360 (1986).
[10]J. N. Schulman and T. C. McGill, Phys. Rev. B **19**, 6341 (1979); Phys. Rev. Lett. **39**, 1680 (1977).
[11]J. N. Schulman and Y. C. Chang, Phys. Rev. B **24**, 4445 (1981); **27**, 2346 (1983).
[12]S. Krishnamurthy and J. A. Moriarty, Phys. Rev. B **32**, 1027 (1985).
[13]E. Caruthers and P. J. Lin-chung, Phys. Rev. Lett. **38**, 1543 (1977); Phys. Rev. B **17**, 2705 (1978).
[14]Wanda Andreoni and R. Car, Phys. Rev. B **21**, 3334 (1980).
[15]M. A. Gell, D. Ninno, M. Jaros, and D. C. Herbert, Phys. Rev. B **34**, 2416 (1986).
[16]J. M. Berroir and T. A. Brum, Superlatt. Microstruct. **3**, 239 (1987).
[17]C. G. Van de Walle and R. M. Martin, Phys. Rev. B **35**, 8154 (1987).
[18]N. E. Christensen, Phys. Rev. B **37**, 4528 (1988).
[19]D. M. Bylander and L. Kleinman, Phys. Rev. Lett. **59**, 2091 (1987); **60**, 472 (1988).
[20]D. M. Wood, S.-H. Wei, and A. Zunger, Phys. Rev. Lett. **58**, 1123 (1987); Phys. Rev. B **37**, 1342 (1988).
[21]S. Ciraci and I. P. Batra, Phys. Rev. B **36**, 1225 (1987).
[22]T. Nakayama and H. Kamimura, J. Phys. Soc. Jpn. **54**, 4726 (1985).
[23]N. Hamada and S. Ohnishi, Superlatt. Microstruct. **3**, 301 (1987).
[24]M. Posternak, A. Baldereschi, S. Massidda, and A. J. Freeman, in *Proceedings of the 14th International Symposium on Gallium Arsenide and Related Compounds, Heraklion, Crete, Greece (1987)*, Inst. Phys. Conf. Ser. No. 91, edited by A. Christou and H. S. Rupprecht (Institute of Physics, Bristol, 1988), p. 537.
[25]P. Hohenberg and W. Kohn, Phys. Rev. **136**, B964 (1964); W. Kohn and L. J. Sham, ibid. **140**, A1133 (1965).
[26]O. K. Andersen, Phys. Rev. B **12**, 3060 (1975).
[27]G. B. Bachelet and N. E. Christensen, Phys. Rev. B **31**, 879 (1985).
[28]D. M. Ceperley and B. J. Alder, Phys. Rev. Lett. **45**, 566 (1980).
[29]J. Perdew and A. Zunger, Phys. Rev. B **23**, 5048 (1981).
[30]N. E. Christensen, Phys. Rev. B **30**, 5753 (1984).
[31]M. S. Hybertsen and S. G. Louie, Phys. Rev. Lett. **55**, 1418 (1985), Phys. Rev. B **34**, 5390 (1986).
[32]N. E. Christensen, E. Molinari, and G. B. Bachelet, Solid State Commun. **56**, 125 (1985).
[33]J. Nagle, M. Garriga, W. Stolz, T. Isu, and K. Ploog, J. Phys. (Paris) Colloq. **5**, C5-495 (1987).
[34]D. S. Jiang, K. Kelting, T. Isu, H. J. Queisser, and K. Ploog, J. Appl. Phys. **63**, 845 (1988).
[35]E. Finkman, M. D. Sturge, and M. C. Tamargo, Appl. Phys. Lett. **49**, 1299 (1986).
[36]M. Garriga, M. Cardona, N. E. Christensen, P. Lautenschlager, T. Isu, and K. Ploog, Phys. Rev. B **36**, 3254 (1987).
[37]M. Kobayashi, T. Toriyama, and Y. Horikoshi, Appl. Phys. Lett. **50**, 1811 (1987).
[38]M. Cardona, T. Suemoto, N. E. Christensen, T. Isu, and K. Ploog, Phys. Rev. B **36**, 5906 (1987).
[39]A. Ishibashi, Y. Mori, M., Itabashi, and N. Watanabe, J. Appl. Phys. **58**, 2691 (1985).
[40]M. Alouani, S. Gopalan, M. Garriga, and N. E. Christensen, Phys. Rev. Lett. **61**, 1643 (1988).
[41]G. F. Koster, J. O. Dimmock, R. G. Wheeler, and H. Statz, *Properties of the Thirty-two Point Groups* (MIT Press, Cambridge, 1963).
[42]R. Sooryakumar, A. Pinczuk, A. C. Gossard, D. S. Chemla, and L. J. Sham, Phys. Rev. Lett. **58**, 1150 (1987).
[43]H. L. Stormer, Z. Schlesinger, A. Chang, D. C. Tsui, A. C. Gossard, and W. Wiegmann, Phys. Rev. Lett. **51**, 926 (1983).
[44]A. Alexandrou, M. Cardona, and K. Ploog, Phys. Rev. B **38**, 2196 (1988).
[45]*Landolt-Börnstein Tables*, edited by O. Madelung, M. Schulz,

and H. Weiss (Springer, Berlin, 1982), Vol. 17a.
[46]See, for instance, G. L. Bir and G. E. Pikus, *Symmetry and Strain-Induced Effects in Semiconductors* (Wiley, New York, 1974), pp. 309ff.
[47]N. F. Johnson, H. Ehrenreich, K. C. Hass, and T. C. McGill, Phys. Rev. Lett. **59**, 2352 (1987).
[48]S. Gopalan, M. Cardona, and N. E. Christensen, Solid State Commun. **66**, 471 (1988).
[49]M. Cardona, N. E. Christensen, and G. Fasol, Phys. Rev. B **38**, 1806 (1988).
[50]Yu. A. Byckov and E. I. Rashba, in *Proceedings of the International Conference on the Physics of Semiconductors,* edited by J. D. Chadi and W. A. Harrison (Springer, New York, 1985), p. 312.